# Building the Runway: A New Superconducting Magnet Test Facility Made for the SPARC Toroidal Field Model Coil

T. Golfinopoulos, P. C. Michael, E. Ihloff, A. Zhukovsky, D. Nash, V. Fry, J. P. Muncks, R. Barnett, L. Bartoszek, W. Beck, W. Burke, W. Byford, S. Chamberlain, D. Chavarria, K. Cote, E. Dombrowski, J. Doody, R. Doos, J. Estrada, M. Fulton, R. Johnson, B. LaBombard, S. Lane-Walsh, M. Levine, K. Metcalfe, C. O'Shea, A. Pfeiffer, S. Pierson, D. K. Ravikumar, M. Rowell, F. Santoro, S. Schweiger, J. Stillerman, C. Vidal, R. Vieira, E. Voirin, A. Watterson, S. Wilcox, M. J. Wolf, and Z. Hartwig

***Abstract*—A new superconducting magnet test facility was created at the MIT Plasma Science and Fusion Center (PSFC) for the SPARC Toroidal Field Model Coil (TFMC) program. The facility was designed and constructed in parallel with the TFMC between 2019 and 2021, with capabilities and design approaches tailored to the needs of this project and its time line. The major components of the facility include a new cryostat (outer dimensions, 5.3 m $\times$ 3.7 m $\times$ 1.5 m) with open bore; a novel cooling system circulating supercritical helium in a closed loop to provide $\sim$600 W cooling power at $\sim$20 bar-a, $\sim$20 K; a 50-kA $\pm$ 10-V power supply with supporting nitrogen-cooled high temperature superconductor (HTS) binary current leads operating at record currents, as well as VIPER-cable HTS cold bus; and a new instrumentation and programmable-logic-controller-based control system handling $\sim$650 input and output signals distributed between the facility and the test article. Substantial legacy infrastructure inherited from the PSFC's Alcator C-Mod tokamak program, including liquid nitrogen facilities and 10 mW of ac power, was instrumental in the rapid deployment of these new systems. Immediately after initial commissioning, the facility was used successfully to test the SPARC TFMC, operating the magnet in a campaign achieving 20 T on the coil, as well as a second campaign performing quench testing. The facility has since undergone several upgrades and has been used in campaigns of other test articles, and it is expected that the facility will remain a resource for the community for the foreseeable future to develop fusion magnets and related technology.**

***Index Terms*—Magnet test facility, high-temperature superconductors, superconducting magnets, tokamak devices, toroidal field model coil, supercritical helium (SHe) cooling, cryostat, SPARC, instrumentation and control.**

Manuscript received 22 September 2023; revised 27 November 2023 and 4 December 2023; accepted 6 December 2023. Date of publication 10 January 2024; date of current version 7 February 2024. This work was supported by Commonwealth Fusion Systems (CFS), under Grant RPP-006, and the parties have pursued patent protection relating to inventions. Commonwealth Fusion Systems has exclusive commercial rights to the technology for energy generation. *(Corresponding author: T. Golfinopoulos.)*

T. Golfinopoulos, P. C. Michael, E. Ihloff, A. Zhukovsky, V. Fry, W. Beck, W. Burke, W. Byford, K. Cote, J. Doody, J. Estrada, M. Fulton, B. LaBombard, S. Lane-Walsh, A. Pfeiffer, S. Pierson, D. K. Ravikumar, M. Rowell, F. Santoro, S. Schweiger, J. Stillerman, C. Vidal, R. Vieira, A. Watterson, and Z. Hartwig are with Plasma Science and Fusion Center, Massachusetts Institute of Technology, Cambridge, MA 02139 USA (e-mail: golfit@mit.edu).

D. Nash, J. P. Muncks, R. Barnett, S. Chamberlain, D. Chavarria, E. Dombrowski, R. Doos, R. Johnson, M. Levine, K. Metcalfe, C. O'Shea, and S. Wilcox are with Commonwealth Fusion Systems LLC, Devens, MA 01434 USA.

L. Bartoszek and E. Voirin are with Bartoszek Engineering, Aurora, IL 60506 USA.

M. J. Wolf is with the Karlsruhe Institute of Technology, 76131 Karlsruhe, Germany.

Color versions of one or more figures in this article are available at https://doi.org/10.1109/TASC.2024.3352395.

Digital Object Identifier 10.1109/TASC.2024.3352395

## I. Introduction

THE SPARC Toroidal Field Model Coil (TFMC) project was an approximately three-year effort between 2018 and 2021 that developed novel rare-earth yttrium barium copper oxide (REBCO) superconductor technologies [1], [2], [3], [4] and then utilized those technologies to successfully design, build, and test a first-in-class high-field ($\sim$20 T) representative scale ($\sim$3 m in linear size) superconducting toroidal field (TF) coil (see Table I). With the principle objective of retiring the design, fabrication, and operational risks inherent in large-scale no-insulation REBCO superconducting magnets for fusion energy devices, the project was executed jointly by the MIT Plasma Science and Fusion Center (PSFC) and Commonwealth Fusion Systems (CFS) as a critical technology enabler of the high-field pathway to fusion energy [5] and, in particular, as a risk retirement program for the TF magnet in the SPARC net energy fusion tokamak [6]. This is one of a collection of papers intended to cover the principal parts of the TFMC project, including the design and fabrication of the magnet, the design and assembly of the test facility, and an overview of the results from the experimental test campaigns carried out in the fall of 2021.

The focus of this article is on the magnet test facility created specifically to support the TFMC experimental campaign. This facility encompasses the electrical and cryogenic services to the magnet, as well as all instrumentation and control (I&C) associated with operation of the facility and characterization of the magnet under test, and all associated facility infrastructure. The facility was built on the site of the former Alcator C-Mod power room and benefited from the features inherited from this previous usage, including 10 mW of 480 $V_{AC}$ power, deionized (DI) water cooling circuit, and a nearby 68 000-L (18 000-gal)

(a) (b)

Fig. 1. (a) C-Mod "Power Room" in late 2019 prior to its transformation into the magnet test facility and (b) the same space in July 2021, just prior to the installation of the TFMC into the main cryostat, shown with the majority of the PSFC and CFS personnel involved in the PSFC project.

TABLE I
TFMC SUMMARY PARAMETERS

| Design Parameter | Value |
|---|---|
| Overall magnet mass | 10,058 kg |
| Overall winding pack size | 2.9 m×1.9 m |
| Winding pack mass | 5,113 kg |
| Winding pack current density | 153 A/mm$^2$ |
| Winding pack inductance | 0.14 H |
| Winding pack ampere-turns | 10.4 MA-turns |
| Terminal current | 40.5 kA |
| Number of turns | 256 |
| Number of pancakes | 16 |
| Total REBCO tape length | 270 km |
| Coolant type | Supercritical helium |
| Coolant pressure | 25 bar-a (max.), 14 bar-a (typ.) |
| Operating temperature | 20 K |
| Peak magnetic field | 20.3 T |
| Peak Lorentz loading | 822 kN/m |
| Magnetic stored energy | 110 MJ |

liquid nitrogen tank. Nonetheless, the construction of this facility represented an enormous undertaking, requiring the design and procurement of entirely new power, cryogenic, instrumentation, control, and rigging systems, as well as the demolition and removal of a substantial amount of legacy equipment. This transformation is depicted in Fig. 1, showing photographs of the cell just prior to and after its reconstruction. The result of this effort is described herein.

The rest of this article is organized as follows. First, background information is presented to provide context for the facility's layout. Principal components are then described individually. Finally, summary remarks are made, with brief mention of the continuing and future use of the facility.

## II. Overview of the Facility

### A. Background

The superconducting magnet test facility was designed and constructed between 2019 and 2021, in parallel with the SPARC TFMC, itself. The long lead times associated with many of the critical components, and the short time scale of the project, forced procurement decisions to be made with a degree of uncertainty, particularly regarding the detailed geometry of the magnet and its interfaces to the facility. The design philosophy relied upon applying conservative assumptions and emphasizing simplicity to help mitigate uncertainty and reduce schedule risk. Nonetheless, a number of design parameters were known at the outset of the project. Among these were the rough dimensions of the magnet, as well as the number of ampere-turns required to achieve $\geq$20 T on the coil while satisfying approximate targets for current and stored magnetic energy density. From this early footprint, the number of joints in the coil was defined; using a conservative assumption of 3–5 n$\Omega$ per joint and estimates of radiant heat load to the device, engineering requirements on the cryogenic system followed. The magnetic moment of the device was also known approximately, from which the field contours influencing facility layout and safety boundaries could be adequately estimated. To motivate the discussion, Fig. 2 provides a computer-aided design (CAD) rendering of the TFMC with helium "plena" at either end, together with a lumped-element model after that in [7]. It is important to keep in mind, however, that the level of detail depicted in CAD rendering was not available at the project outset; rather, the data collated in Table II are more representative of the initial design inputs, together with the circuit model in Fig. 2(b).

Nonetheless, these parameters were sufficient to begin procurement activities for both the helium cryogenic plant and the magnet dc power supply—the two longest lead items in the facility.

### B. Time Line of Facility Preparation

The time line of this reconfiguration was as follows: initial design work began in July 2019, leading to long-lead procurement beginning in the autumn of 2019. The floor space was cleared of power components between January and August, 2020, during which time the facility was closed for roughly three months due to the COVID pandemic. The helium cryoplant and the 50 kA dc power supply were delivered, installed, and commissioned between August and December 2020. The gantry

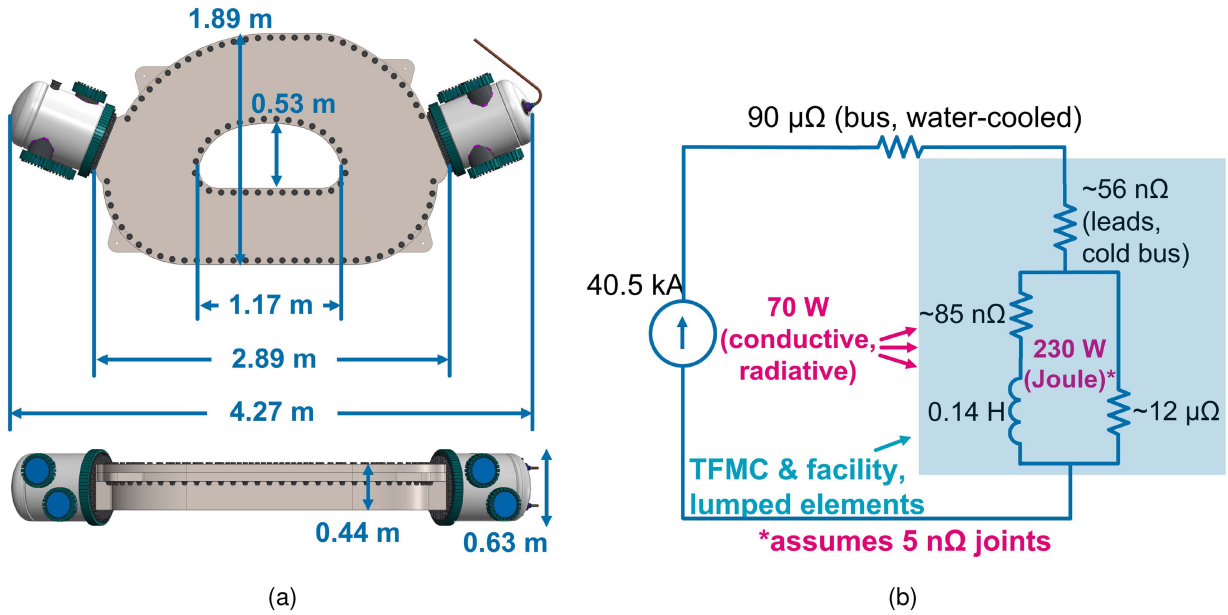


Fig. 2. (a) Rendering of the TFMC with dimensions; this detailed depiction of the coil was not available at the start of the project. (b) Simplified lumped-element model after that in [7] depicting basic electrical and thermal parameters of the TFMC and facility—this model was available almost from the outset of the project. The parallel legs of the TFMC represent the azimuthal and radial current paths, including joints and neglecting voltage drop in the superconductor.

TABLE II
FACILITY DESIGN CONSIDERATIONS

| Parameter | Description |
|---|---|
| Voltage/dump requirements | Low voltage, no dump resistor |
| Fringe fields | 5 G (0.5 mT) line at 16.4 m, 30 G (3 mT) line at 9 m |
| Cooling Power | $\sim$ 600 W cooling power at $\lesssim$ 20 K |
| Instrumentation | Voltage, temperature, field, and flow measurements made inside high pressure, low-temperature envelope |
| Control | All-remote operation, PLC-based control hardware, real-time data views with 100's signals |

crane was installed in January 2021, the main cryostat in March 2021, the water-cooled bus in April 2021, the current leads in May 2021, the nitrogen lines between March and May 2021, and the radiation shields and vacuum-jacketed helium transfer lines in June 2021. I&C systems were deployed throughout the spring of 2021, with substantial development and procurement before this time. Major components—the dc power supply, the cryocooler arrays, the modular components of the current leads, and the crane—were first commissioned individually. Then, the vacuum system and nitrogen-cooled radiation shields were commissioned together in June 2021. Finally, a full system commissioning was completed in July 2021, in which the current leads and cold bus were cooled to 20 K and operated at 40.5 kA—the expected operating current of the TFMC. The TFMC was installed shortly afterward, with 20 T reached and exceeded on the coil on September 5, 2021, after a first attempt in August 2021 that was aborted due to a helium leak in the instrumentation conduit junction.

### C. Summary of Major Components

The major components of the magnet test facility, and their layout, are shown in an overall photograph in Fig. 3 and CAD renderings in Fig. 4. These components may be grouped within the cryogenic systems, power systems, I&C systems, and basic facility infrastructure, noting that the boundaries of these groupings are overlapping and somewhat arbitrary. The first category—the cryogenic systems—includes the vacuum vessel, nitrogen-cooled radiation shields, vacuum system, cryogenic helium loop, vacuum-jacketed and unjacketed in-vessel helium transfer lines, and nitrogen transfer lines. The power system comprises the 50 kA power supply, water-cooled bus, current leads, and cold bus. The I&C category describes the sensors, signal chains, conditioning electronics, data acquisition modules, programmable logic controllers (PLCs) and associated input and output modules, human–machine interfaces (HMIs), databases, and associated software and hardware. Finally, facility infrastructure here describes the DI water and ac electrical services, 15-ton gantry crane, and safety monitoring systems. These systems are described severally below.

Numerous interfaces exist between these components, and between the facility components and the TFMC. These include vacuum and high-pressure feedthroughs, control feedback loops to maintain desired operating conditions in cryogenic systems, and rigging setups to install and extract the TFMC and other heavy components. They are described in the context of individual systems.

## III. CRYOGENICS SYSTEM

The cryogenics system comprises all the components necessary to bring the magnet, cold bus, and current leads—a cold mass of over $\sim$10 t ($\sim$11 short tons)—to their desired operating temperatures of $\sim$20 K.

Fig. 3. Photograph of the PSFC Superconducting Magnet Test Facility, as it appeared at the conclusion of TFMC testing in December 2021. The SPARC TFMC appears in the lower-right-hand corner of the photograph.

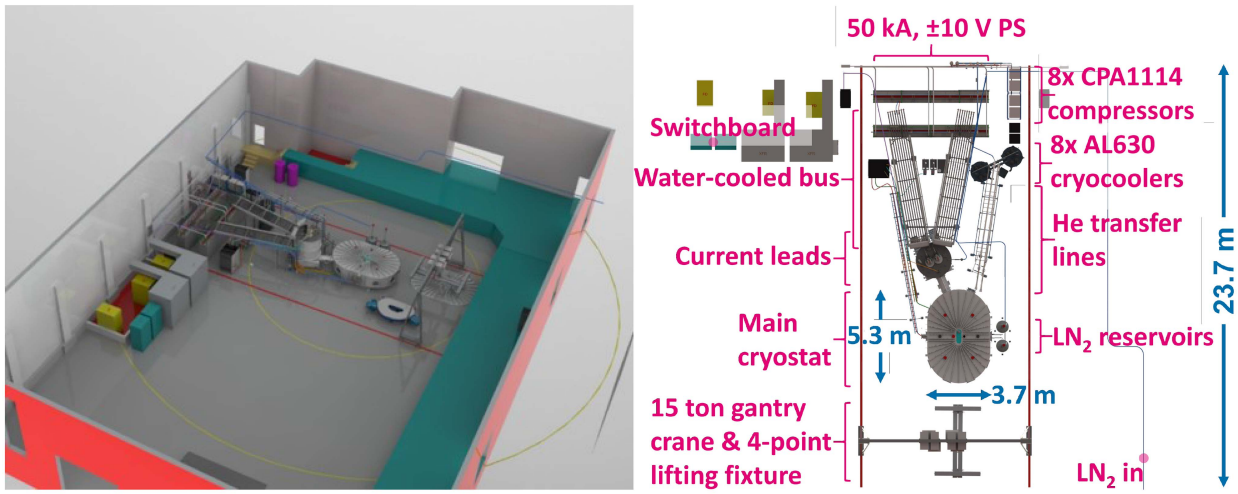


Fig. 4. (a) CAD rendering of the facility with 30 and 5 G (3 and 0.5 mT) lines shown in gold. It should be noted that the entirety of the area at $\geq$5 G is within walled-off locations on-site that are inaccessible to the public. (b) Top-down view of the facility, as rendered in CAD, with scale and locations of major systems indicated.

In particular, the cryogenics system includes:

1) the vacuum vessel and associated components;
2) the liquid-nitrogen-cooled radiation shields with multi-layer insulation;
3) the liquid-nitrogen cooling system for the current leads;
4) the closed-loop supercritical helium circuit.

This section is meant to summarize the overall system architecture, design specifications, and system interfaces. A detailed accounting of the helium circuit is provided in the article by Michael et al. [8] in this series, and of the cooling of the current leads in [9], with measurements from operation appearing in [10].

### A. Vacuum Vessel

Fig. 5 shows an image of the main vacuum vessel, as well as a CAD rendering cutaway. Its interior volume is roughly 15.3 $m^3$ (539 $ft^3$). The geometry of the main vessel was largely constrained by the need to fit the TFMC footprint with substantial margin, as well as to accommodate the relatively shallow head room (3.12 m, 123 in) of the newly installed gantry crane. It

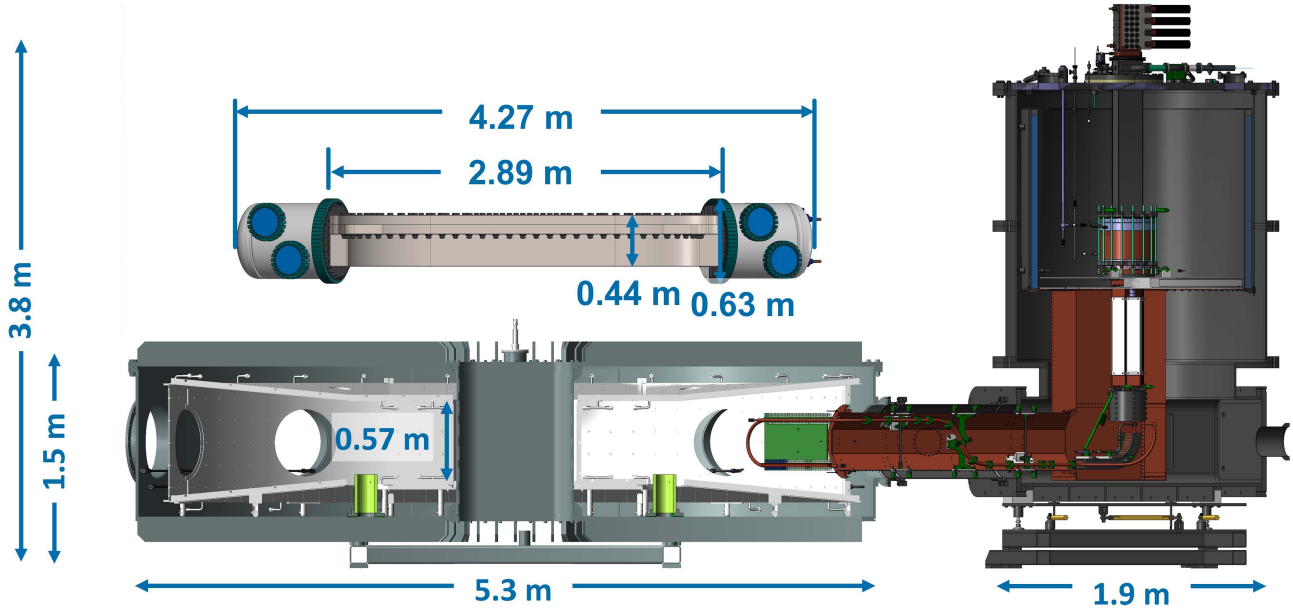


Fig. 5. Cutaway CAD rendering of cryostat and coil, annotated with key dimensions. The current leads are on the right-hand side of the figure.

is constructed of dual-certified 304/304 L stainless steel and weighs 13 800 kg (30 400 lbs). It was manufactured by Anderson Dahlen, Inc., Ramsey, MN, USA, between May 2020 and March 2021.

The topology of the vessel, with its open-air bore at room temperature, was motivated by the desire to install highly accurate air-only diagnostics—in particular, a fiber-optic current sensor and magnetic field sensors. The central internal support also halves the otherwise long span of the nondished lid from end to end. Future use of the facility also considers a flexible space in which to insert test samples in a strong background field.

The design of the vessel is consistent with the American Society of Mechanical Engineers (ASME) Boiler and Pressure Vessel Code, particularly [11, Sec. VIII], with the following criteria.

1) The yield strength for the dual-certified SS304/SS304L is taken as 172 MPa (25 ksi).
2) The allowable membrane stress is $P_m < \sigma_a = \frac{2}{3}\sigma_y =$ 115 MPa (16.67 ksi).
3) For membrane and bending stress, $P_m + P_b < \frac{3}{2}\sigma_a = \sigma_y =$ 172 MPa (25 ksi).
4) For membrane and bending and secondary stress, $P_m + P_b + Q < 3\sigma_a = 2\sigma_y =$ 345 MPa (50.1 ksi).

Finite-element analysis showed the design to satisfy these constraints under gravitational and atmospheric loading at ∼100 kPa-d (15 psi-d), as well as internal loading at ∼200 kPa-d (30 psi-d). Fig. 6 shows a plot of exaggerated deflection resulting from this finite-element method (FEM) analysis, with a maximum deflection of ∼1.6 mm (∼0.0635 in) occurring at the middle of the longest span of the lid. An analysis of bolt shear was also performed. The bending of the sidewalls is significant, and some plastic deformation was observed after initial operation, causing the hole pattern to become misaligned between the side walls and the lid at the midspan. A cam tool was then made to return the holes to alignment.

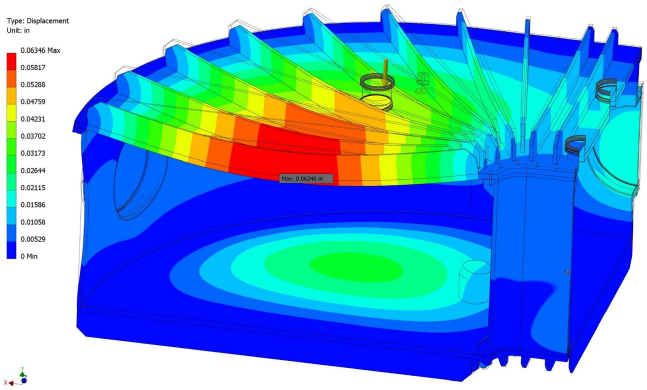


Fig. 6. FEM analysis of the main vacuum vessel showing exaggerated deflection, with a maximum deflection of ∼1.6 mm (∼0.0635 in) occurring at the middle of the most eccentric axis.

Three relief valves are placed on the vessel, two on the main vessel and one on the lid of the current-lead cryostat. These open at 20 kPa-g (3 psi-g) and are meant to deploy in the event of a sudden loss of cryogen inside the vacuum, which could result in overpressure of the device.

All vacuum seals on the vessel are of fluoropolymer. In steady operation, vacuum pressures of $\lesssim 10^{-3}$ Pa ($\lesssim 10^{-5}$ torr) are typically achieved once the moisture is removed by the application of nitrogen cooling on the radiation shield; vacuum pressures of $\lesssim$70 $\mu$Pa ($\lesssim 5 \times 10^{-7}$ torr) are typical with the advent of cryopumping from the helium circuit, typically operating at <30 K. At these vacuum pressures, residual gas heat transfer to the TFMC was negligible.

The current lead vacuum vessel is attached to the main vacuum vessel via the bus tunnel and shares the same vacuum, adding

another ∼5 $m^3$ to the vacuum space for a total volume of ∼20 $m^3$. It consists of three sections—two stacked cylindrical sections bolted together at 2.032-m (80-in) outer-diameter (OD) flanges and a rectangular-section base of outer dimensions, 1.844 m× 1.621 m (72.6 in × 63.8 in), with four large flat flanges upon which additional small flanges are readily added. This structure rests on a tube-stock support and may be moved and rotated in-plane with a set of turnbuckles. The overall height of the assembly, from the floor to the lid, is 3.302 m (130 in), but the current leads protrude an additional 0.533 m (21 in) above the lid. The vessel was manufactured by Vacuum Plus Manufacturing, Inc., Chelmsford, MA, USA.

### B. Radiation Shields

Radiation shields are used in the main cryostat, the current lead cryostat annex, and the bus tunnel between them. The shields in the main cryostat consist of 24 separate panels: six on the top, six on the bottom, 10 around the outer perimeter, and two around the inside. The current lead cryostat shields consist of an annular $LN_2$ reservoir surrounding the vapor-cooled copper portions of the binary current leads, beneath which is affixed a copper sheet metal assembly thermally bonded to the reservoir and conduction-cooled. The bus tunnel shield is also of copper sheet metal construction with hexagonal section, coming in two halves, which are also thermally bonded to the main cryostat's outer thermal shields and conduction-cooled.

The radiation shields of the main chamber were manufactured by Anderson Dahlen, the same manufacturer as the main cryostat. After drawing sign-off, production lasted approximately three months. They form a stainless steel bladder constructed of two 3.2-mm (1/8-in-thick) sheets of 304 stainless steel suspended over an 3.2-mm (1/8-in) gap by welded plug spacers. There are over 1100 such spacers, and they are, themselves, spaced 152.4 mm (6 in) apart from one another. The resulting assembly is mechanically robust and able to support the weight of workers walking over the surface. The panels rest upon a set of legs formed from 304 stainless steel tube stock with G10 hemispherical inserts for contacts to the floor of the cryostat.

The upper and lower radiation shields are given a ∼5° slope to help separate evolving nitrogen vapor from liquid and to aid in controlling fill level. Along the inner diameter (ID), the shield panels have vertical separation of ∼584 mm (∼23 in). Cutouts in the shields give access to the ten side ports and eight ports on the cryostat lid; the side panels are made such that each end straddles half a port. These cutouts are covered with overlapping copper half-circles conduction-cooled from their curved perimeters.

The panels are gravity-fed on two circuits by two external reservoirs. The first circuit ties together the bottom, inner, and top panels; the second circuit ties together all ten outer panels. The plumbing is run such that the manifold does not complete a full loop around the vessel, but has a split so as to disrupt eddy currents induced by rapid collapse of the TFMC's magnetic field during quench. Both reservoirs are fed from a single vacuum-jacketed feed line that ultimately ties into the facility's 68 000-L (18 000-gal) storage tank outside the building. The feed system for the radiation shields is described in more detail in Section III-D.

All of these radiation shields are covered on all sides by a 25-layer multi-layer insulation (MLI) blanket, as seen in Fig. 7. The blanket was manufactured by Aerospace Fabrication, Farmington, MN, USA, and comprises an assembly of multiple sheets precut to be form-fitting to the radiation shield panels and their ports. The total area covered by all sheets was ∼63 $m^2$ (∼680 $ft^2$). The goal of the blanket was to reduce nitrogen evolution rates in the shields and to limit temperatures in the conduction-cooled copper sections of radiation shields around the bottom of the current leads and through the bus tunnel. The total expected radiant heat over all radiation shield surfaces without a blanket might be estimated around 5 kW; the lower emissivity of the MLI may reduce this roughly 20-fold, dropping $LN_2$ consumption rates due to this heat source from a value on the order of ∼100 L/h to ∼1–5 L/h.

The blankets were initially affixed to the stainless steel walls of the shield panels with dual-lock strips. The strips were anchored by plastic T-tags on the blanket side, but relied on the clear acrylic adhesive backing of the strips to hold the blankets in place on the panels. This acrylic failed at cryogenic temperatures during commissioning, so the blankets were subsequently supported with vacuum-compatible tie line.

The helium circulation system's cryostats, separate from the main cryostat, also have their own radiation shields consisting of aluminum sheet with copper tracer line, surrounded with five layers of MLI. These were nitrogen-cooled during the 20-T TFMC campaign, but allowed to operate dry in the subsequent quench test campaign, as the extra heat leak was deemed acceptable, and it was considered more desirable to avoid added issues of condensation and icing with the nitrogen flow.

### C. Vacuum System

Two water-cooled Leybold Model 1000 turbomolecular pumps are responsible for pumping down the cryostat, each with a nominal pumping speed of 1000 l/s for He, a gas throughput of 7 mbar-l/s (5.25 torr-l/s), and an ultimate pressure of $10^{-10}$ mbar ($7.5 \times 10^{-11}$ torr). These draw through the current lead vacuum vessel via a short conduction path through tubes terminated by DN200CF flanges (OD 254 mm, 10 in) and are isolated by pneumatically driven gate valves. Their location allows them to be situated as far as possible from the bore of the magnet while still having a short conduction path to the vacuum vessel. The peak field from the TFMC at this location is ∼14 mT; this is nominally within the pumps' field rating, but ferromagnetic shields were placed around the pumps to further protect them. The assembly is depicted in Fig. 8.

Each of the two turbo pumps is backed by a separate Leybold Ecodry 35 Plus multistage root pump with a nominal pumping speed of 35 $m^3$/h (1240 $ft^3$/h) and ultimate pressure of $10^{-2}$ mbar (7.5 mtorr).

At present, the cryostat contains no provision for bake-out. Instead, moisture reduction is accomplished by three "pump-purge" cycles in which the vessel is pumped down to ∼1 torr, back-filled with dry nitrogen gas to atmospheric pressure, and then pumped down again. Fig. 9 shows the pump-down from the TFMC quench campaign, with a typical set of pump–purge cycles lasting two to three days.

Fig. 7. Installation of the final panel of the main cryostat radiation shield prior to the 20-T campaign. The TFMC is visible underneath. MLI blankets cover the exterior surface of the radiation shield, including ports.

Fig. 8. Photograph of the two turbo pumps and gate valves attached to the back of the current lead cryostat annex.

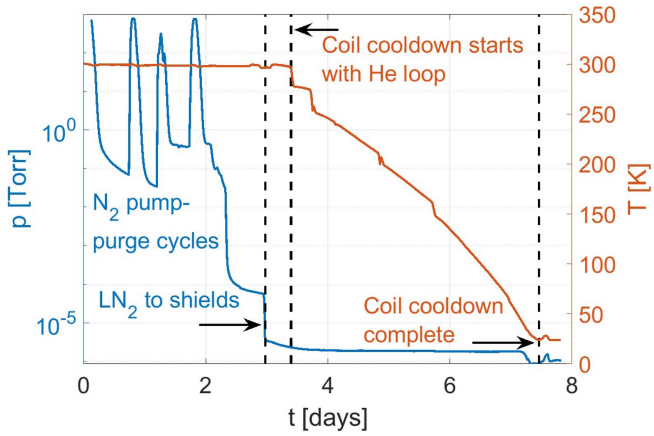


Fig. 9. Pump-down of the TFMC during the quench campaign in October 2021; the blue line shows the vacuum pressure in the main cryostat, while the orange line shows the temperature of helium entering the coil.

### *D. Liquid Nitrogen Feed System*

The test facility had access to an 68 000-L (18 000-gal) liquid nitrogen storage tank adjacent to the experimental cell, inherited from the former operation of the Alcator C-Mod tokamak; another nearby 26 500-L (7000-gal) tank offered auxiliary storage. Vacuum-insulated transfer lines already communicated nitrogen to the building interior. New jacketed lines from the Vacuum Barrier Corporation, Woburn, MA, USA, extended this service to the cell. The largest of these is a run of S-10 Semiflex that is ∼39.6 m (130 ft) long, with OD 76 mm (3 in) and ID 36 mm (1.4 in). This line terminates at a phase separator, where the feed is split into three parallel S-5 triax lines of total length 36.6 m (120 ft), each with OD 51 mm (2 in) and ID 17 mm (0.66 in). The shortest of these feeds the tracer around the shields of the cryocooler arrays, the longest feeds the two reservoirs on the main cryostat shields, and the remaining line feeds the outer shield/reservoir of the binary current leads.

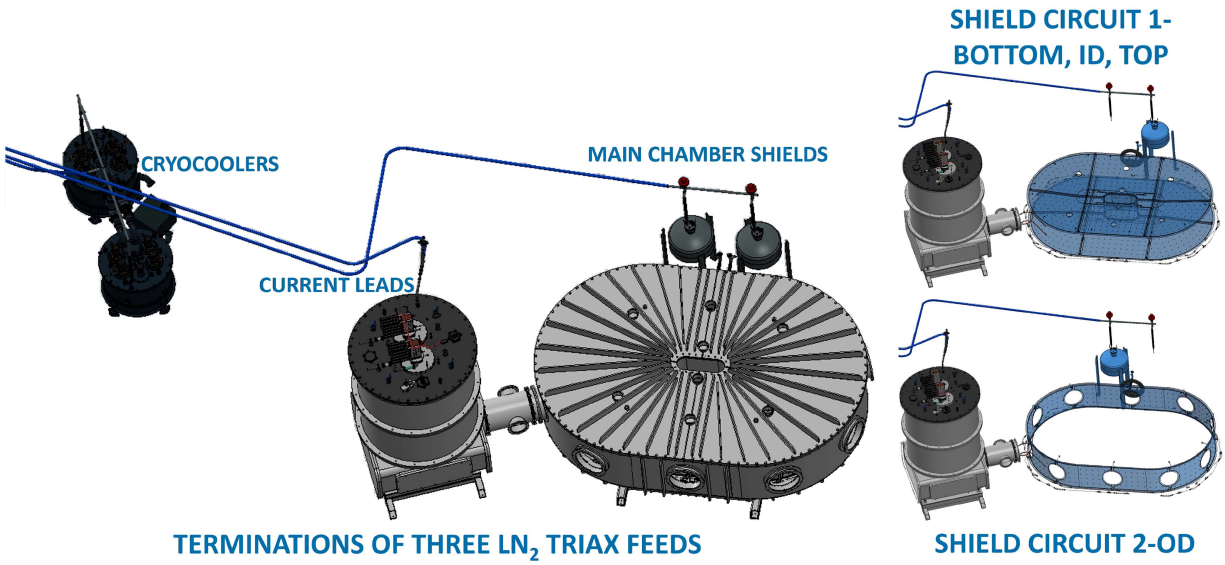


Fig. 10. CAD rendering around the terminations of the three $LN_2$ triax lines: the cryocooler arrays, the current lead shield/reservoir, and the reservoirs of the main cryostat shields. Detail views show how the main cryostat shield panels are connected, with one reservoir feeding the side panels on the OD, and the other feeding the panels on the bottom, ID, and top.

Fig. 10 illustrates a close-up around the destinations of these three triax lines and how the shield panels of the main cryostat are plumbed. The panels on the bottom, ID, and top (shield circuit 1) are gravity-fed from one reservoir, while those along the OD draw nitrogen from the other reservoir (shield circuit 2). The liquid supply and vapor exhaust manifolds connecting the panels are of rigid and flexible stainless steel tube terminated with Swagelok VCR fittings using copper gaskets. They extend clockwise and counterclockwise around the cryostat from the flange beside the reservoirs, but do not complete a circuit in order to provide an electrical break to suppress eddy currents. The supply manifolds are at the bottom of the shields, and the exhaust at the top.

Nitrogen vapor from the main cryostat shields in the steady state is exhausted out of the cryostat lid; it is then run along a heat exchanger and is released to the ambient air. Nitrogen consumption of the main shields after cooldown is on the order of 1 L per hour, which does not present a significant oxygen deficiency hazard to the cell.

Nitrogen consumption from the current leads, when idling after cooldown, is roughly 20 times greater. The vapor is drawn into a nearby flexible duct of diameter 0.3 m (12 in) with a blower fan. The cold temperatures around the nitrogen exhaust lines can condense water onto surfaces, especially on humid days with high dew point; depending upon operating conditions, some water may freeze on surfaces. To mitigate this issue, and especially to prevent freezing, warm air is blown over these surfaces to raise their temperature. A dry enclosure is expected to be fitted in the future.

Nitrogen vapor evolution from the cryocooler arrays is relatively small; direct exhaust from the tracers is heated and released to the ambient air. It should be noted that the radiation shields of the cryocooler arrays were not used during the TFMC quench campaign, as the heat leak was sufficiently small. The nitrogen line was then redirected to an activated-charcoal cold trap installed in the compressed helium gas feed to the cryocoolers.

Nitrogen vapor at the phase separator is exhausted from the building through an outdoor vent heater.

In the reservoirs of the main cryostat and current leads, capacitive level sensors from American Magnetics, Inc. are used in conjunction with the AMI 1700 liquid level control instrument, with pneumatic valves regulating the flow. Two-position ON/OFF valves are used everywhere except for the boiling chambers of the current leads, which employ continuous flow control valves manufactured by WEKA AG. A number of manual valves are also present to enable and disable flow to and within the facility at the start and end of a campaign.

Additional details on the liquid nitrogen system for the current leads may be found in the article by Fry et al. [9] in this series.

TABLE III
HELIUM SYSTEM DESIGN PARAMETERS

| Parameter | Value |
|---|---|
| Nominal supply temperature | 18 K |
| Maximum allowable working pressure (MAWP) | 28 bar-a |
| Maximum Expected Operating Pressure (MEOP) | 20 bar-a |
| Test pressure under He | 31 bar-g |
| He flow rate | $\geq$50 g/s |
| Cooling capacity | 600 W |

### *E. Supercritical Helium Circuit*

The supercritical helium circuit is responsible for cooling the coil, the cold bus, and the bottom-most section of the current leads. It is described in detail in the article by Michael et al. [8] of this series; here, a summary is provided. Under nominal conditions, joint heating is the dominant heat load to the circuit, with heat leak due to radiation, conduction, and residual gas heat transfer all of smaller order. Table III summarizes the high-level design parameters of the system. The system chosen to satisfy

(a) (b)

Fig. 11. (a) Two arrays of four Cryomech AL630 cryocoolers in assemblies by Absolut System; also visible are the supply and return tees connected to the He transfer lines and the vacuum pumps pulling on the Absolut cryostats and (b) Two control racks—one for each array—and eight Cryomech CPA-1114 compressors that drive the cryocoolers.

these requirements is a closed-loop helium circuit circulating supercritical helium past arrays of cryocoolers. These arrays, as well as the transfer lines that link them to the cold mass, are described as follows.

*1) Cryocooler Arrays:* The cryocooler array concept had already been demonstrated as a flexible simple-to-maintain cryogenic cooling platform with minimal helium usage [12], [13] and was selected over an open-loop liquid helium proposal, as well as a closed-loop scheme that would have employed a refurbished cryogenic refrigerator. The topology employed here is as follows: two separate modules of four cryocooler arrays are arranged in parallel. Each module has four Cryomech AL630 cryocoolers, arranged in two parallel legs, each with two cryocoolers in series. A single cryogenic circulation fan upstream of these legs drives flow through each module. The assemblies were designed and manufactured by Absolut System, Seyssinet-Pariset, France; Absolut also furnished a control rack for each module, as well as custom cryofans, and tees to interface to the transfer lines. Fig. 11 shows photographs of the completed assembly as installed in the facility, as well as the eight Cryomech CPA-1114 compressors that drive the cryocoolers.

Coarse temperature regulation may be achieved by enabling or disabling particular compressors; fine regulation is accomplished via heaters affixed to the cold heads, with ∼300 W available in each of the two arrays. The heaters feed back against a temperature reading at a downstream cold head.

*2) Transfer Lines and Internal Routing:* The vacuum-jacketed transfer lines communicate supercritical helium between the cryocooler arrays and the cryostat. This allows for adequate standoff between the arrays and the magnet, with the cryogenic equipment situated in sufficiently low fringe field, ≤3 mT (30 G), at maximum operating current in the TFMC.[1]

Two 10.5 m (34 ft 5 in) vacuum-jacketed helium transfer lines, sourced from PHPK Technologies, Columbus, OH, USA, couple the cryocooler arrays to the main cryostat. Interfaces to tees on the cryocooler end and to the feedthroughs on the cryostat end are made with sliding-bell joints. The vacuum of each line is independent from that of the main and cryocooler cryostats and is normally not pumped. The cold helium lines inside the vacuum jacket are covered with a 22-layer MLI blanket to limit heat leak. A pair of manual shut-off valves provides isolation between the transfer lines and the main vacuum vessel to permit magnet installation and removal without exposing the rest of the helium circuit to atmosphere.

Inside the main vacuum vessel, unjacketed transfer lines route helium to and from the coil, relief valves, and cold bus. These were fabricated mainly from Cryoworks, Inc., Jurupa Valley, CA, USA. The lines generally have ID ≥38 mm (≥1.5 in) and consist of both rigid and flexible sections. During the TFMC campaigns, a fraction of the helium exhaust was used to cool the cold bus, with the remainder bypassing the bus and running directly to the return line. An orifice was welded inside the return line to effect this flow division.

The circuit is relieved via two large relief valves set to trip at 26.5 bar-a (370 psi-g), a safety measure meant to protect the system from overpressure events. These are coupled to flanges on the inlet and outlet plena and feeding vertically out the lid of the cryostat to prevent strong convective heat leak. The circuit may be vented manually at these relief valves or remotely by a solenoid valve placed outside the 30 G line.

## IV. Instrumentation and Control System

The I&C system monitors and controls roughly 650 input and output signals. Of these, 315 are embedded inside the coil pressure boundary, 57 are on the coil case surface, and the remainder are distributed around the facility, both inside and outside of the vacuum vessel. Measured quantities include voltage, current, temperature, pressure, flow, field, strain, pH, $O_2$ concentration, and several other facility state conditions.

Facility I&C is concerned primarily with regulating the operating conditions in accordance with the experimental plan, as well as maintaining a safe and secure work environment. The primary goal of instrumentation in and on the coil is to

[1]The advice of the manufacturer was that the cryocooler arrays should be placed in a field ≤5 mT (50 G); additional margin was added, allowing future operation of magnets with greater fringe fields than the TFMC.

characterize the coil performance in support of the project physics mission. However, there is significant overlap between the instruments employed to carry out these two tasks, and the distinction between "facility" and "coil" instrumentation is based as much on geography as use case.

In the following, the I&C system is summarized, noting that more detailed information on particular sensors and associated equipment is provided in the subsystem articles pertaining to the coil [14] and its operation [10], as well as the helium circuit [8], and current leads [9].

### A. Facility I&C Systems

Facility measurements are generally meant to interface to a real-time control system via a PLC architecture built around the Siemens SIMATIC S7-1500 series and compatible hardware. A variety of analog and digital cards provide up to 128 digital and 176 analog inputs, as well as 64 digital and 12 analog outputs, of which about three quarters are in use. These are used to monitor voltage, temperature, pressure, door and Kirk key interlock sensors, as well as water flow measurements, and also serve the nitrogen- and water-cooled systems.

Additional devices interface to the PLCs via Ethernet communication. Among these are two Lake Shore F71 Teslameters coupled to three-axis FP Hall probes mounted on the lid of the main cryostat; a Condis electronic fiber-optic current transformer (EFOCT) measuring the bus supply current and the azimuthally flowing current within the coil; liquid nitrogen level measurements made using capacitive sensors into the American Magnetics, Inc., Model 1700; a large number of cryogenic temperature measurements recorded on Cryocon 18i monitors offering real-time calibration; and an Oxigraf oxygen monitoring system with four sensors.

The EFOCT merits particular attention, as it is the primary current measurement device, offering 0.2% precision or better, and being immune to inductive pickup. Two fibers are available, each with active length of ∼20 m. One of these completes seven turns around the supply bus near the positive current lead terminal. The other links the coil through the open bore with a single turn and measures the azimuthally flowing current, allowing direct decomposition of the radial and azimuthal current components. The maximum current reading is only 400 kA-turns, above which the polarization angle exceeds the measurable range, and therefore, the sensor was not available over the entire ramp to $>$ 10 MA-turns. It was, therefore, used to calibrate the three-axis Hall probes at low current as an auxiliary azimuthal current measurement. However, the system's polarization angle sweeps around a full 360° roughly every 2 MA-turns; this meant that the angle wrapped back in range during the flattop currents in both the 20-T campaign at 40.5 kA ($\leq$10.37 MA-turns) and the quench campaign at 31.5 kA ($\leq$8.06 MA-turns).

The Ignition platform, made by Inductive Automation, provides the Supervisory Control and Data Acquisition environment, with the open-source `InfluxDB` database utility as its historian. This is run on a pair of redundant servers. Data and control interfaces are displayed in a graphical HMI on a pair of personal computers; data can also be viewed in customizable dashboards using Grafana data visualization software.

TABLE IV
EMBEDDED DEVICES

| Description | Count |
|---|---|
| Voltage tap pairs | 205 |
| Hall sensors, HGCT-3020 | 4 |
| Temperature sensors, CX-1070 | 34 |
| Flow sensors, FS2 | 34 |
| Quench heaters | 4 |

### B. TFMC Embedded and Case Instrumentation

Table IV catalogs by type the I&C devices embedded within the TFMC case: 277 measurements, as well as four quench heaters deployed on the coil, but never used. Examples of embedded instrumentation devices are also depicted in the photographs of Fig. 12. The primary mission of the embedded instrumentation was to characterize the performance of the coil and validate model predictions regarding:

1) critical current and transition;
2) azimuthal and radial distribution of current;
3) joint resistances;
4) quench initiation and propagation;
5) thermohydraulic performance.

The secondary mission of the instrumentation was to provide data at a ∼30 s update rate for operators to gauge slow-moving trends in the coil and adjust control inputs accordingly.

Voltage taps were the most numerous embedded sensor variety, characterizing coil and joint performance in normal and off-normal conditions. These were made using a novel printed circuit board, referred to as the "instrumentation board," that was laid into helium cooling channels around the exhaust plenum. This offered a demountable instrumentation platform providing a consistent and well-located sensor layout, as well as convenient, rapid, and relatively low-risk installation process during winding pack stack-up. A long thin projection of the board followed a cooling channel to track from the OD to the ID of the coil, crossing each turn of the pancake. Spring contacts projected from the surface of the board to the copper caps below, ensuring adequate compliance while also securing the board in-place within each channel. Varied pairings of the voltage taps were conveniently made on the boards and brought to separate twisted pairs within cable harnesses. Six pancakes in critical locations had higher measurement density, with all nearest neighbor turn-to-turn voltages resolved, as well as overall voltages. Voltage measurements on the remaining pancakes skipped turns to reduce the overall pin count while still tracking voltage everywhere on the coil.

Four Hall sensors, Lake Shore Model HGCT-3020, were installed at the top, bottom, and middle of the pancake stack in the tight-corner regions of the ID. These were driven using a current-spinning technique to reduce the impact of the planar Hall effect [15]. The nominal goals of these sensors were to help constrain azimuthal and radial current components and peak field on the coil, and to offer a fast-resolution field sensor to track current collapse after quench onset. They were bonded to the cooling channel surface with Stycast epoxy and wired to termination pads on the instrumentation boards.

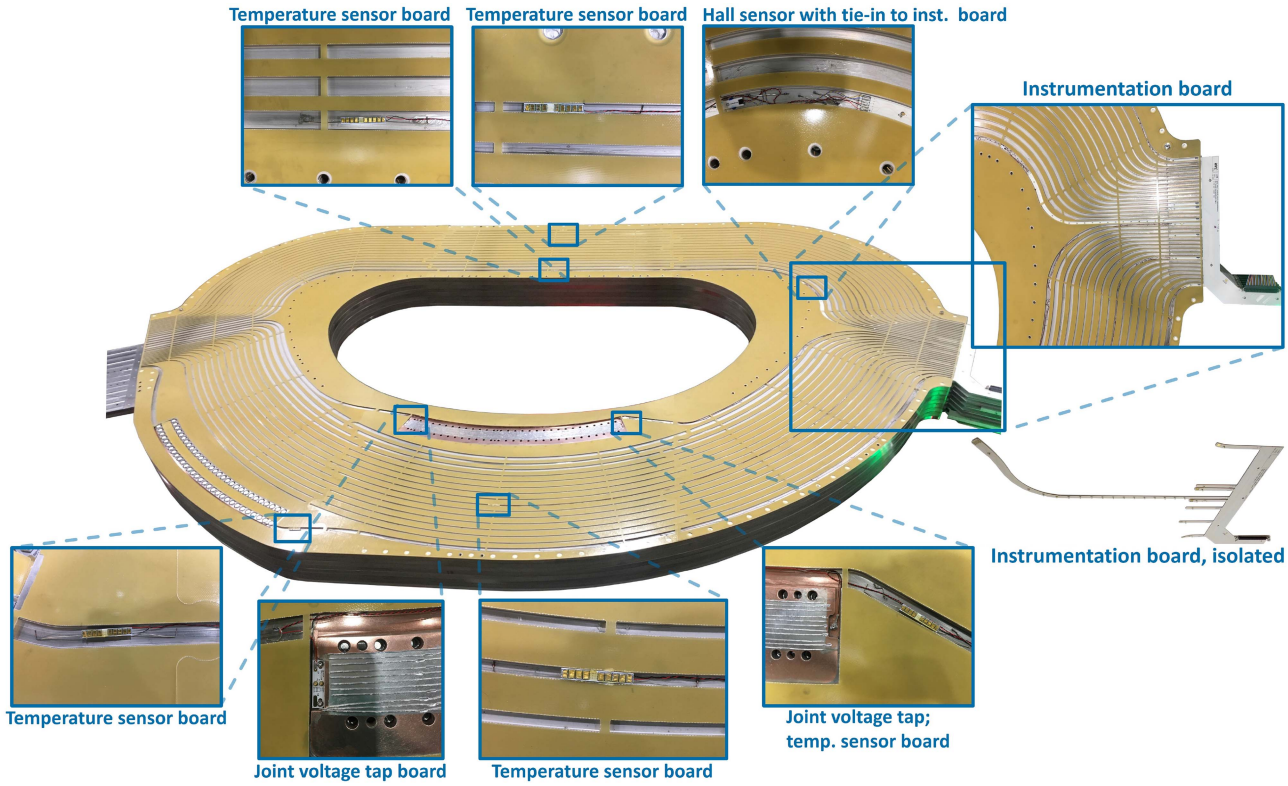


Fig. 12. Examples of embedded instrumentation arrayed upon a pancake on the coil midplane.

Thirty-four temperature and 34 helium flow sensors were distributed across the coil cross section to help gauge thermohydraulic performance. This was especially important due to the fact that helium flow was not strictly constrained in the coil, being supplied and exhausted at large plena at either end of the device, and dividing according to the varied width and length of the 528 flow channels and additional flow paths for case cooling. Thermohydraulic models of varying complexity were used to estimate this flow division and resultant cooling capacity, and these measurements were sought to validate the model results. The available sensors were disposed to create as representative a picture as reasonable, given the impracticality of providing measurements along each of the large number of flow paths.

Temperature measurements were typically placed across the coil section of maximum coil width, i.e., the approximate mirror symmetry plane of the "D"-shaped coil, with additional measurements made near the joints. They were accomplished using Lake Shore Cernox 1070 RTDs in the SD package. To facilitate sensor integration during winding pack assembly, these devices, too, were affixed to a small circuit board mounted within the flow channel. Spring contacts on one side of the board pressed thermal pads on the other side onto the copper caps of the opposing pancake, with a layer of Apiezon-N grease used to ensuring adequate thermal contact. Wires were then run within the cooling channel to termination pads on the instrumentation boards.

Flow measurements were made using the Innovative Sensor Technology FS2 device. These devices were affixed on the instrumentation board in a variety of flow channels of varying widths. The operating principle of these devices is to perform a calorimetric measurement of heat convected along the chip, made possible by a sophisticated set of signal conditioning electronics.

Embedded signals were collected in the outlet plenum and routed to bundles of cable harnesses via a flexible printed circuit "landing board." They then needed to transit both the thermal and pressure boundary between the interior of the coil and the exterior of the vacuum vessel. These two tasks were separated, following the general approach pursued on the Large Hadron Collider [16]. A thermal intercept, made from expanding foam, envelops each of two copper signal line bundles at the outlet plenum of the TFMC, interrupting helium convection from the cold mass. The lines were then run through 63.5-mm-ID ($2\frac{1}{2}$-in-ID) flexible conduits to the feedthroughs, as shown in Fig. 13(b). Here, 50-pin D-sub feedthroughs manufactured by MPF Products, Greenville, SC, USA, were welded into a customized thickened version of the EVAC NW200 CeFiX blank. The feedthroughs, themselves, were rated to ~50 bar-a (~750 psi-a) and 500 V. The CeFiX NW200 flange was designed for a maximum allowable working pressure (MAWP) of 28 bar-a, with testing using pressurized helium at 31 bar-g. Ten feedthroughs were welded into each blank, as shown in Fig. 13(a), making a total of 1000 pins available. A total of 774 were used in the TFMC experiments.

The cable harnesses within the conduits consisted of bundles of 4 m (~13 ft 1.5 in) long 0.2 mm-diameter (32-AWG) Teflon-shielded copper wire. This corresponded to a total copper area of 24.3 $mm^2$ and a heat leak due to the conduction of less than 1 W.

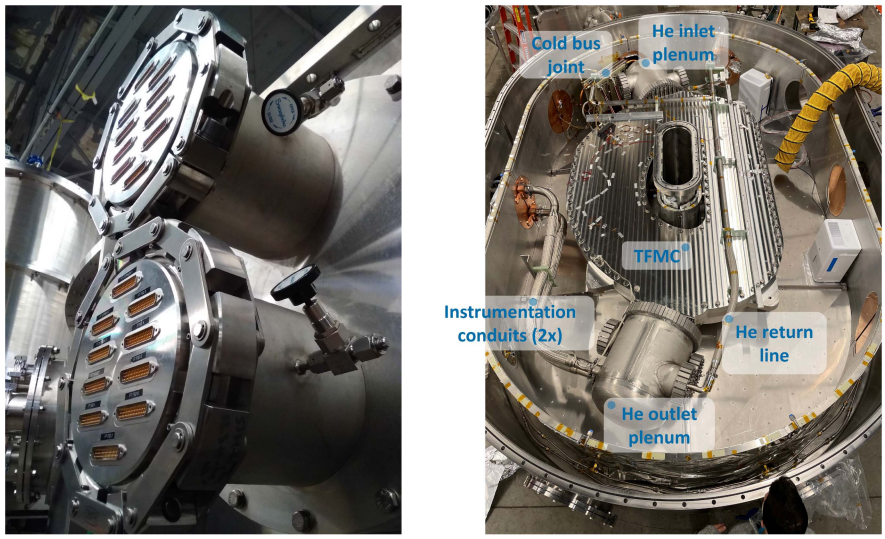


Fig. 13. Photographs of (a) the two high-pressure feedthroughs serving embedded devices and (b) the TFMC situated within the vacuum vessel. The helium flow path in the return line runs from the bottom to the top of the photograph.

Data acquisition for most embedded devices was supplied by a set of four modules manufactured by D-TACQ Solutions, Ltd., Glasgow, U.K.. Three of these devices provided two-stage amplifiers with remotely programmable gain and 24 bits of resolution, totaling 288 channels. These were used to monitor voltage taps. The remaining module provided an additional 96 channels, measuring between $\pm$ 10 V without amplification and serving the field and flow measurements. These devices all recorded at a sampling rate of 1250 Hz and were tightly synchronized. The data so recorded are archived using an `MDSplus` open-source database.

Temperature measurements were recorded separately using Cryocon 18i monitors, recorded in the `InfluxDB` database.

An additional nine Cernox temperature sensors were placed on the case of the TFMC. The primary function of these devices was to monitor the cooldown of the coil, but, given their azimuthal and vertical disposition around the coil, they also helped to constrain temperature gradients during steady-state operation. Redundant sets of strain gauges were deployed to measure both azimuthal and vertical components of strain. Including "dummy" measurements that were not bonded directly to the coil surface, a total of 12 gauges were deployed. These were measured using two VPG Micro Measurements Model 8000-8-SM data acquisition systems operating as a half-bridge.

## V. DC Power System

The low-voltage dc power system is responsible for delivering dc service to the winding and comprises the power supply, room-temperature bus, cryogenic current leads, and cryogenic superconducting bus. The high-current and low-voltage specification characteristics were driven by the needs specific to the TFMC project. In particular, it is noteworthy that that no high-speed dump circuit was included in the original system, since the noninsulated TFMC acted as its own permanent dump resistor. Such components are intended for future upgrades to the facility, however, and are in production as of the writing of this publication.

### A. 50-kA Power Supply

The 20-T-on-tape design target of the TFMC led to a maximum expected operating current of 40.5 kA—this was established by magnetostatic calculations made in July 2019. The 50-kA specification of the supply finally procured was motivated by the desire to achieve both margin for the TFMC and flexibility for future use of the facility. A 48-pulse thyristor-based $\pm$ 10-V supply was selected to satisfy this requirement. Manufactured by Alpha Scientific Electronics, subsequently reincorporated into Magwatt, LLC, the device is very similar to the supply deployed on the ITER Central Solenoid Module test facility [17]. It consists of eight cabinets, each serviced by 480-V three-phase power, with sequential phase shifts between cabinets of 22.5°. The device is water-cooled and typically operates with a total flow of $\sim$450–470 L/min (120–125 gal/min) across all cabinets.

### B. Water-Cooled Bus

The water-cooled bus carries current between the dc power supply and the cryogenic current leads. The power supply was located beyond the 3 mT (30 G) line at 9 m (29.5 ft) from the coil dipole center in order to prevent fringe fields from affecting its operation, and this provided the primary constraint on the bus length. Moreover, essentially all of the voltage drop in the system occurs in the water-cooled bus. In order to regulate accurately, the power supply requires a sufficiently large load voltage, suggested as $\gtrsim$3 V at full current by the manufacturers, setting an approximate design target of $\gtrsim$75 $\mu\Omega$ for the total resistance of

Fig. 14. Photograph of 16 water-cooled bus lines newly arranged on stand, prior to installation of plumbing; supply and return for each cabinet are adjacent.

TABLE V
RIGID BUS PARAMETERS

| Parameter | Value |
|---|---|
| Round-trip length | 15 m (49'2") |
| ID | 26 mm (1.023") |
| OD | 50 mm (1.969") |
| Cu Current density, 40.5 kA/50 kA | 3.53 A/mm$^2$ / 4.36 A/mm$^2$ |
| Material | Luvata OFE-OK® OFHC Cu |
| Number of parallel paths | 8 |
| Insulation | PVC 2" Sch 40 |
| Nominal effective resistance | $\sim 25\ \mu\Omega$ |

TABLE VI
FLEXIBLE BUS CABLES

| Parameter | Value |
|---|---|
| Round-trip length | 12.2 m (40') |
| Number of parallel paths | 8 |
| Area/line | 507 mm$^2$ (1000 MCM) |
| Cu Current density, 40.5 kA/50 kA | 9.99 A/mm$^2$ / 12.3 A/mm$^2$ |
| Nominal effective resistance | $\sim 52.5\ \mu\Omega$ |

the bus, and further constraining the bus geometry. The as-built system has a whole-circuit resistance of 85–90 $\mu\Omega$. With a steady-state operating current of 40.5 kA, this corresponds to a heat load of 140 kW dissipated within the bus that must be extracted by continuous cooling; this increases to $\sim$210 kW at 50 kA. This is a challenging heat load to accommodate via passive air cooling, but is readily removed using the DI water-cooling infrastructure already available in the facility.

The bus topology chosen connected each cabinet to the current leads via an independent supply and return line in order to maximize standoff between cabinets and improve regulation, per the recommendation of the power supply manufacturer.

The bus constructed to meet these constraints consists, for each of the supply and return paths, of a 7.5 m (24 ft 7 in) rigid section joined to 3.1 m (10 ft) flexible lines attached at either end. The rigid section is constructed from 5-m-long pieces of extruded copper sourced from Luvata, Pori, Finland; a single braze joins these on each path. The flexible sections are sourced from Watteredge, LLC. All other interfaces are bolted. A total of 16 lines—eight supply and eight return—are thus formed.

Tables V and VI summarize bus parameters, while Fig. 14 shows the water-cooled bus lines newly installed upon their aluminum stand, prior to the attachment of plumbing.

### C. Binary Current Leads

The binary current leads developed for the TFMC facility are covered in detail in the article by Fry et al. [9] in this article series. However, a brief overview is given here to place the leads in the wider context of the facility.

The existing liquid nitrogen infrastructure at the center, combined with the limited time available to complete the project, led to the selection of a binary lead scheme combining a vapor-cooled copper upper section and a high-temperature superconducting lower section. These meet at a liquid nitrogen boiling chamber, whose exhausted nitrogen vapor cools the copper upper section, while cooling the lower HTS section via conduction. The geometry of this arrangement is depicted in the annotated sectioned CAD rendering of Fig. 15. Not shown in this assembly is the multilayer insulation blanket that covers the exterior of the radiation shield.

During TFMC operations, the boiling chamber was maintained at roughly atmospheric pressure; however, a set of claw pumps connected to the exhaust circuit can reduce pressure in the boiling chamber below atmospheric, thereby subcooling the boiling nitrogen temperature to $\lesssim$70 K.

The geometry of the interface between the current leads and the cold bus is seen in Fig. 16. The lower end of each lead is terminated in a demountable joint to the cold bus, wherein a short piece of VIPER cable [1] slides into a sleeve formed by the closure of six copper segments brazed to the HTS carriers. These six "petals" are compressed onto the VIPER cable by

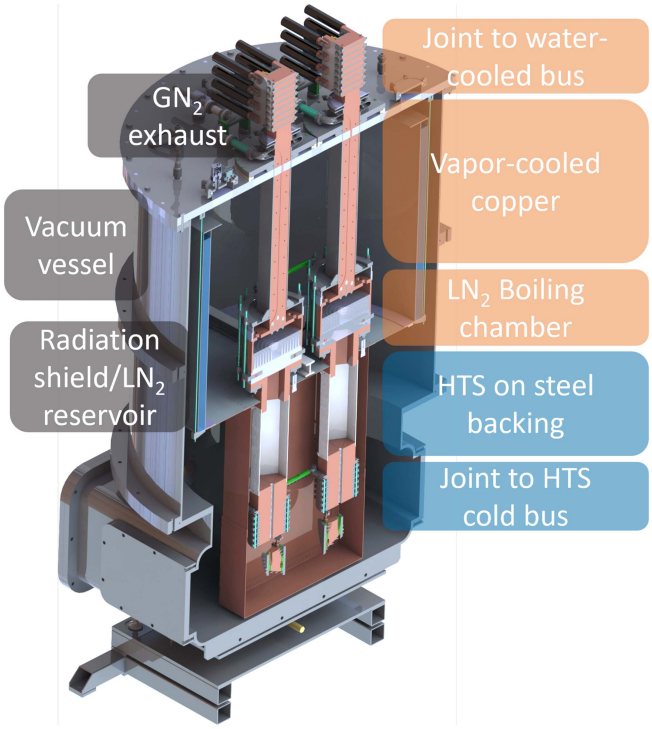


Fig. 15. Section view of binary current leads, showing the normal and superconducting regions of the assembly.

bolts driving from a cylindrical stainless steel strong-back; this VIPER cable then joins to the cold bus across a copper saddle. The bottom of the current lead is conduction-cooled through the joint to the cold bus and operates near the helium circuit temperature. Thermal standoff between the ∼20 K helium circuit and the ∼77 K boiling chamber is accomplished by the stainless steel backing of the HTS tapes, separating the boiling chamber and cold bus joint by 0.48 m (18.9 in).

The overall resistance of each lead is ∼750 nΩ, localized primarily in the upper part of the lead.

### D. Superconducting Cold Bus

The cold bus provides dc electrical service between the cryogenic current leads and the TFMC. Constructed of VIPER cable [1], the bus was designed to exceed the needs specific to the TFMC; hence, adequate REBCO tape was employed for operation at the full rated current of the power supply, 50 kA, at a temperature in excess of 40 K, providing for flexibility and margin beyond the 40.5 kA operating current at 20 K needed by the TFMC.

Table VII lists parameters of the cold bus assembly. At the current-lead end of the cold bus, the bus is jointed to a short VIPER cable extension via a curved saddle. This cable extension, in turn, mates to the six-petal sleeve at the base of the current lead.

Fig. 16 shows a CAD rendering cutaway of the cryostat around the cold bus tunnel. On the right of the figure is the current lead cryostat annex, with the positive current lead shown and the negative lead hidden. The positive and negative cold bus lines run alongside one another to the left. They separate upon entering the main cryostat, where they meet extensions from the TFMC. This bend aids the bus in accommodating thermal contraction. Fig. 17 shows a photograph looking down the bus tunnel from the main cryostat toward the current leads.

TABLE VII
COLD BUS PARAMETERS

| Parameter | Value |
|---|---|
| Length | 4.30 m (pos.), 3.27 m (neg.) |
| OD/$J_e$ at 50 kA | 21.3 mm (0.84 in)/140 A/mm$^2$ |
| ID/He flow rate | 10 mm (0.394 in) / ∼ 10 g/s per bus |
| Spacing/Load at 50 kA | 41 mm (1.614 in) / 12 kN/m (900 lbs-f/ft) |
| Nominal $I_c$ | 60 kA at 45 K |

## VI. FACILITY INFRASTRUCTURE

### A. AC Electrical Service

Sited in the former Alcator C-Mod power room, the magnet test facility has significant electrical capacity. 10 MW of 480 $V_{AC}$ three-phase power is available via two 5-MW substations. One of these two stations serves the 50-kA power supply. With a requirement of 1500 A of 480 $V_{AC}$ three-phase (∼1.25 MW), this power supply represents the largest load on the system. A new 2000-A Square-D switchboard backing ten new 200-A breakers allows for the isolation of the system during maintenance.

The balance of the system runs from the second substation; here, the biggest load is from the eight CPA-1114 compressors, sinking a total of ∼104 kW, requiring ∼125 A of 480 $V_{AC}$ three-phase service.

### B. Cooling Water System

A DI chilled water loop was inherited from the Alcator C-Mod tokamak [18] facility. New conduits and manifolds were installed in the test cell to connect to the existing set of pumps. The system can deliver $\gtrsim$176 gal/min ($\gtrsim$666 L/min) to service the magnet test facility; this is divided between the eight cabinets of the 50-kA power supply (∼125 gal/min, 473 L/min), the eight cryocooler compressors (∼27 gal/min, 102 L/min), the eight supply and return pairs of the room-temperature bus (∼23 gal/min, 87 L/min), and the vacuum turbo pumps (∼1 gal/min, ∼4 L/min). Heat is exchanged to a chilled water line provided by the MIT Central Utilities Plant.

The pH on the system is moderated by a series of neutralizing ion exchange resin bead tanks; this system typically maintains the pH between 6.5 and 7, although the higher temperatures (with the bus reaching or exceeding 35 °C) associated with 50-kA operation tend to push the pH down to 6.25. A higher pH of 7.5–8.5 is preferable to reduce the rate of corrosion on the numerous copper surfaces on the water loop [19], particularly in the compressors and power supply, while the water's conductivity is minimized at a pH of 7 [19], noting that higher voltage operation is expected in coming campaigns. pH control in the facility is, hence, a subject for future optimization.

Water pressure, temperature, and flow rate are monitored continuously for discrete subsystems, with permissive locks in

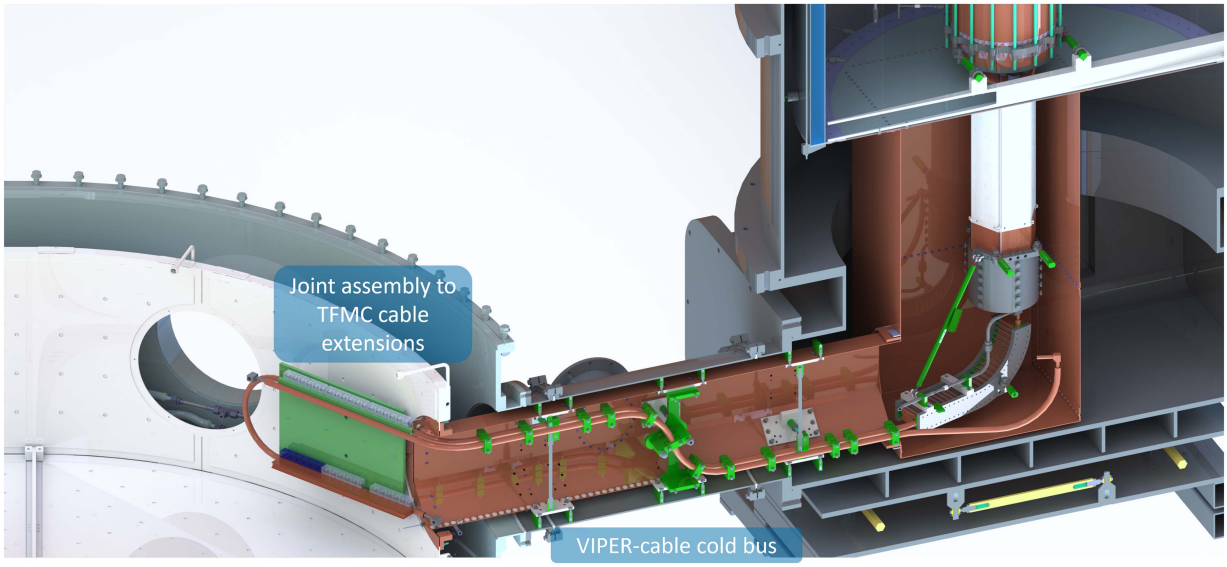


Fig. 16. CAD rendering of both cold bus lines. One current lead is shown, together with its interface to the cold bus. A cutaway of the joint assembly to the TFMC bus extensions is shown at the other end.

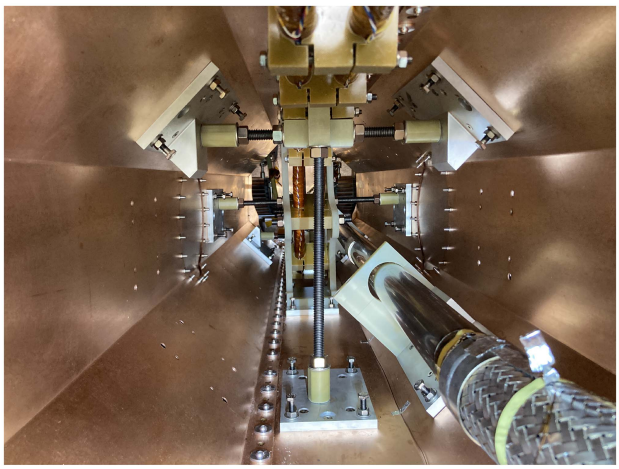

Fig. 17. Photograph looking down the cold bus tunnel from the main cryostat into the current lead cryostat annex. The cold bus runs from the top and center of the photograph down along the center of the bus tunnel, while the helium return line runs along the bottom-right.

the control system to prevent equipment start-up if cooling water is not within nominal parameters.

Process water temperature is typically set to 21.1 °C (70 °F). During the TFMC's 20-T campaign, the process temperature floated up to 22.8 °C (∼73 °F), as the heat load on the cooling loop at peak current reached ∼405 kW, exceeding the ∼350 kW regulation compliance capacity of the existing heat exchanger. The heat exchanger has subsequently been upgraded, with a new capacity of 835 kW at nominal operating conditions, and the entire facility commissioned with dc power supply output at 50-kA operation for many thermal equilibration times.

The copper terminals at the top of the current leads are serviced by a separate water circuit driven by a Budzar heater/chiller unit.

### C. Gantry Crane

A new Spanco 15-short-ton (13.6 t) gantry crane was installed in order to place and remove the coil, as well as the cryostat lid, radiation shield panels, and other heavy pieces of equipment. The overall height of the crane is 5.22 m (17 ft $1\frac{1}{2}$ in), giving it 38 mm (1.5 in) clearance from the overhead roof joists. When fully retracted, the gantry crane hook height is 3.12 m (123 in) above the floor, while the edge of the top of the main cryostat flange, with lid off, is 1.38 m (54.3 in), leaving 1.74 m (68.7 in) head room above the cryostat. An adjustable Harrington four-point lifting fixture rated to 15 short tons was used to install the magnet into the cryostat, taking up a further 0.402 m (15.81 in) in height from bale to shackle. If 0.46 m (18 in) is consumed by lifting straps, and 10 cm (4 in) by lifting eyes, this leaves an effective maximum sample height of ∼0.78 m (∼30.6 in). The TFMC, at a maximum height of 0.63 m, cleared this minimum with roughly these parameters.

Moreover, given that the bottom of the winding pack case sat 1.084 m (42.68 in) above the facility floor, the lifting straps and eyes needed to have a vertical extent of $\geq$0.38 m (15 in) to prevent the lifting fixture from interfering with the center column. This condition was also satisfied.

The spreader beam, itself, weighs approximately 1360 kg (3000 lbs), meaning that the maximum sample weight is 12 250 kg (27 000 lbs) when the spreader beam is used. At 10.06 t (22 170 lbs), the TFMC was under this limit.

## VII. Conclusion

A new superconducting magnet test facility was created at the MIT PSFC in support of the SPARC TFMC project. The facility was designed and built in two years, in parallel with the magnet, itself. All-new cryogenic, power, instrumentation, control, and rigging equipment was developed, installed, and

integrated, taking advantage of the facility's existing infrastructure, including substantial power, water, and nitrogen services. The development activity began in July 2019 and concluded in July 2021 with the successful commissioning of the cryogenic and power systems, reaching the TFMC nominal operating current (40.5 kA) and temperatures (20 K with 20 bar-a He). The TFMC was tested immediately afterward, with the 20-T campaign running in August and September 2021 and the quench campaign in October and November 2021.

Since the completion of TFMC testing, the facility has been upgraded, adding additional I&C infrastructure to the current lead, cold bus, power supply, and cryogenic systems, and roughly doubling the cooling capacity of the water-cooling system. This enabled the facility's use in two additional campaigns: one for commissioning the binary current leads to their design value of 50 kA, and one in support of the SPARC Central Solenoid Model Coil. It also demonstrates the versatility and flexibility of the facility, with adaptations readily integrated into the base infrastructure.

In the near future, the facility will continue to support SPARC magnet development, receiving upgrades to add dump resistors with fast discharge up to ∼100 V and, later, auxiliary pulsed-power systems. It will also become available to host varied testing campaigns to further the development of fusion magnet technology and related fields.

## Acknowledgment

A large number of people contributed to the success of the TFMC project, in general, and the creation of the test facility, in particular, often under difficult circumstances during the COVID-19 pandemic. The authors would like to thank all of those involved. The authors particularly extend their gratitude to S. Agabian, D. Arsenault, J. Burrows and D. Bellofatto, V. Censabela, J. Chicarello, C. Cotta, J. Irby, J. James, A. Q. Kuang, S. Kuznetsov, R. Landry, G. MacKay, K. Moazeni, J. Mota, A. Radovinsky, R. Rosati, W. Saunders, M. Silveira, P.W. Stahle, T. Toland, D. Tracey, D. Whyte, and B. Wood of the PSFC, J. Kelsey of Bates Research and Engineering Center, J. Hollman, R. Mumgaard, and B. Sorbom of Commonwealth Fusion Systems, W. Fietz of the Karlsruhe Institute of Technology, J. Tanchon and the team at Absolut System, W. Sherman and J. Sullivan and the team at Magwatt LLC (formerly Alpha Scientific Electronics), S. O'Connell and F. Stenzel and the team at Anderson Dahlen, S. Golden and J. Gordon and the team at New England Orbital Services, W. McGrath and Vacuum Plus Manufacturing, C. Hoyer at CryoWorks, S. Rose at Bode Equipment Company, and S. Gomes at Toupin Rigging Company. The magnet technology in the TFMC Program was developed under research collaborations between MIT and Commonwealth Fusion Systems. The parties have pursued patent protection relating to inventions. CFS has exclusive commercial rights to the technology for energy generation.

## References

[1] Z. S. Hartwig et al., "VIPER: An industrially scalable high-current high-temperature superconductor cable," *Supercond. Sci. Technol.*, vol. 33, no. 11, Oct. 2020, Art. no. 11LT01, doi: 10.1088/1361-6668/abb8c0.

[2] E. E. Salazar et al., "Fiber optic quench detection for large-scale HTS magnets demonstrated on VIPER cable during high-fidelity testing at the SULTAN facility," *Supercond. Sci. Technol.*, vol. 34, no. 3, Feb. 2021, Art. no. 035027, doi: 10.1088/1361-6668/abdba8.

[3] V. Fry, J. Estrada, P. C. Michael, E. E. Salazar, R. F. Vieira, and Z. S. Hartwig, "Simultaneous transverse loading and axial strain for REBCO cable tests in the SULTAN facility," *Supercond. Sci. Technol.*, vol. 35, no. 7, May 2022, Art. no. 075007, doi: 10.1088/1361-6668/ac6bcc.

[4] B. LaBombard et al., "Grooved, stacked-plate superconducting magnets and electrically conductive terminal blocks and related construction techniques," U.S. Patent 11, 417, 464, Aug. 16, 2022.

[5] D. Whyte, "Small, modular and economically attractive fusion enabled by high temperature superconductors," *Philos. Trans. Roy. Soc. A, Math., Phys. Eng. Sci.*, vol. 377, no. 2141, 2019, Art. no. 20180354.

[6] A. J. Creely et al., "Overview of the SPARC tokamak," *J. Plasma Phys.*, vol. 86, no. 5, 2020, Art. no. 865860502.

[7] S. Hahn, D. K. Park, J. Bascunan, and Y. Iwasa, "HTS pancake coils without turn-to-turn insulation," *IEEE Trans. Appl. Supercond.*, vol. 21, no. 3, pp. 1592–1595, Jun. 2011.

[8] P. C. Michael et al., "A 20-K, 600-W, cryocooler-based, supercritical helium circulation systemfor the SPARC toroidal field model coil program," *IEEE Trans. Appl. Supercond.*, vol. 34, no. 2, Mar. 2024, Art. no. 0600113.

[9] V. Fry et al., "50 kA capacity, nitrogen-cooled, demountable current leads for the SPARC toroidal field model coil," *IEEE Trans. Appl. Supercond.*, early access, Jan. 16, 2024, doi: 10.1109/TASC.2024.3354237.

[10] D. G. Whyte et al., "Experimental assessment and model validation of the SPARC toroidal field model coil," *IEEE Trans. Appl. Supercond.*, vol. 34, no. 2, Mar. 2024, Art. no. 0600218.

[11] *SME Boiler and Pressure Vessel Code*, Amer. Soc. Mech. Eng., New York, NY, USA, 2015. [Online]. Available: https://www.asme.org/codes-standards/bpvc-standards

[12] S. Pamidi, C. H. Kim, J.-H. Kim, D. Crook, and S. Dale, "Cryogenic helium gas circulation system for advanced characterization of superconducting cables and other devices," *Cryogenics*, vol. 52, no. 4, pp. 315–320, 2012.

[13] T. Trollier, A. Ravex, J. Tanchon, and J. Lacapere, "20 K cryogenic helium forced flow circulation loop," in *Proc. Int. Cryocoolers Conf.*, 2016, vol. 19, pp. 547–556.

[14] R. Vieira et al., "Design, fabrication, and assembly of the SPARC toroidal field model coil," *IEEE Trans. Appl. Supercond.*, early access, Jan. 22, 2024, doi: 10.1109/TASC.2024.3356571.

[15] I. Ďuran, S. Entler, M. Kohout, M. Kočan, and G. Vayakis, "High magnetic field test of bismuth Hall sensors for ITER steady state magnetic diagnostic," *Rev. Sci. Instrum.*, vol. 87, no. 11, Oct. 2016, Art. no. 11D446, doi: 10.1063/1.4964435.

[16] D. Bozzini, "The standard instrumentation feedthrough system for the LHC cryomagnets," *IEEE Trans. Appl. Supercond.*, vol. 12, no. 1, pp. 1269–1271, Mar. 2002.

[17] K. Schaubel, A. Langhorn, S. Lloyd, Z. Piec, E. Salazar, and J. Smith, "The ITER Central Solenoid Module final test facility," *Fusion Eng. Des.*, vol. 124, pp. 59–63, 2017.

[18] M. Greenwald et al., "20 years of research on the Alcator C-Mod tokamak," *Phys. Plasmas*, vol. 21, no. 11, 2014, Art. no. 110501, doi: 10.1063/1.4901920.

[19] R. Dortwegt and E. Maughan, "The chemistry of copper in water and related studies planned at the advanced photon source," in *Proc. Part. Accel. Conf.*, 2001, vol. 2, pp. 1456–1458.